Cell-Surface MuSK Self-Association: a Crucial Role for the Putative Signal Sequence†

Michael J. Bianchetta,‡,§ Rebecca A. Betensky,|| and Jonathan B. Cohen*,‡

Department of Neurobiology and Harvard University Graduate Program in Neuroscience, Harvard Medical School, 220 Longwood Avenue, Boston, Massachusetts 02115, and Department of Biostatistics, Harvard School of Public Health, 677 Huntington Avenue, Boston, Massachusetts 02115

Received August 3, 2005; Revised Manuscript Received October 7, 2005

ABSTRACT: The receptor tyrosine kinase MuSK plays a crucial role—both as a signaling molecule and structurally—in the process of clustering nicotinic acetylcholine receptors at the neuromuscular junction. Immunofluorescence microscopy of transiently transfected fibroblasts has been used to visualize the cell-surface distribution of MuSK, which is found in discrete, punctate clusters. This distribution does not result from targeting of MuSK to identified plasma membrane subdomains, and MuSK's association with itself is specific, as MuSK clusters at the cell surface are segregated from clusters of other cotransfected receptor tyrosine kinases. A mutational analysis, using coexpressed pairs of MuSK mutants and chimeras, demonstrates that the putative signal peptide is both necessary and sufficient for association with MuSK. Removal of the intracellular domain or most of the extracellular domain, or replacement of the transmembrane domain, does not abolish MuSK self-association. The N-terminus of the MuSK protein, however, is sufficient to recruit another receptor tyrosine kinase to MuSK clusters. Quantitation and statistical analysis of the amount of colocalization between coexpressed MuSK mutants and chimeras confirm these results.

At the mature neuromuscular junction (NMJ),[1] a highly morphologically and molecularly specialized postsynaptic apparatus ensures efficient synaptic transmission (*1*). Nicotinic acetylcholine receptors (nAChRs) are concentrated to over 10 000/μm^2 at the NMJ (*2*), a density at least 3 orders of magnitude higher than the nAChR concentration in extrasynaptic membrane (*3*). During development, nAChRs are evenly and diffusely distributed over the entire cell surface of the developing muscle membrane until innervation (*4*), at which time existing nAChRs in the sarcolemma are recruited to, and anchored at, the site of nerve contact. This clustering is stimulated by the neuronally released, extracellular-matrix associated heparan sulfate proteoglycan agrin (*5*). Deletion of the neuronal-specific agrin gene in mice is lethal, and mice null for this splice variant have fewer, mislocalized nAChR clusters and none of the postsynaptic specializations associated with mature NMJs (*6*).

The agrin receptor consists of the receptor tyrosine kinase (RTK) MuSK (for *Mus*cle-*S*pecific *K*inase) (*7*), coupled with an as-yet unidentified coreceptor, referred to as MASC (for *M*uscle *A*ccessory *S*pecificity *C*omponent) (*8*). Stimulation of MuSK signaling by agrin is in part responsible for reorganization of nAChRs (*9*−*11*), although the sequence of events leading from MuSK phosphorylation/activation to nAChR clustering is still poorly understood (see ref *12* for review).

Interestingly, in addition to the regulation of signaling pathways through its kinase enzymatic activity, MuSK also seems to play a structural role at the NMJ. A trkC−MuSK chimera that is constitutively active but does not contain the MuSK extracellular domain does not induce nAChR clustering (*13*). Similarly, the juxtamembrane region of the MuSK extracellular domain is required for MuSK interaction with the intracellular nAChR clustering protein rapsyn. MuSK has been suggested to function as a central scaffold around which the rest of the postsynaptic apparatus is constructed via interactions with rapsyn (*14*). This theory is supported by the fact that, in mice with a deletion of either the agrin or rapsyn gene, MuSK protein is concentrated in the central innervated band of the muscle membrane despite the lack of synaptic nAChR clustering (*15*). MuSK is concentrated at the adult NMJ (*7*), specifically at the tops of the NMJ secondary folds where both nAChR and rapsyn are also concentrated (*16*). It is not clear to what extent MuSK's function is affected by its localization, but it is has been shown that the functions of other receptor tyrosine kinases are regulated by their compartmentalization in certain membrane subdomains, such as lipid rafts (*17*), caveolae (*18*), and endocytotic machinery (*19*).

In transfected cells, the subset of MuSK in the plasma membrane at the cell surface is clustered. MuSK clusters

† This work was supported in part by USPHS Grant NS18458 (J.B.C.) and a Howard Hughes Medical Institute Predoctoral Fellowship (M.J.B.).

* Address correspondence to Jonathan Cohen. Tel., 617-432-1729; fax, 617-734-7557; e-mail, Jonathan_Cohen@hms.harvard.edu.

‡ Department of Neurobiology, Harvard Medical School.

§ Harvard University Graduate Program in Neuroscience, Harvard Medical School.

|| Department of Biostatistics, Harvard School of Public Health.

[1] Abbreviations: A488, Alexa Fluor 488; A596, Alexa Fluor 596; MuSK, muscle-specific kinase; nAChR, nicotinic acetylcholine receptor; NMJ, neuromuscular junction; rMuSK, rat MuSK; RTK, receptor tyrosine kinase; TM, transmembrane; tMuSK, *Torpedo* MuSK.

10.1021/bi051549j CCC: $30.25 © 2005 American Chemical Society
Published on Web 11/17/2005

with itself but not other coexpressed proteins. To identify structural domains involved in this self-association, which may relate to the structural component of MuSK function, we examined the surface distribution of a panel of MuSK mutants in transfected fibroblasts using immunofluorescence microscopy. Similar experiments have provided information as to the domains of the MuSK protein required for kinase signaling (*20*), agrin binding (*21*), and interaction with rapsyn (*14*). Here, we report that, surprisingly, the putative signal sequence of MuSK is both necessary and sufficient for MuSK self-association and discuss the implications of this finding.

MATERIALS AND METHODS

Antibodies. The antibodies used and their sources are rabbit anti-caveolin, Transduction Laboratories (BD Biosciences); mouse anti-c-erbB-4 H4.77.16, NeoMarkers; mouse anti-clathrin heavy chain Ab-1, Oncogene; mouse anti-Flag octapeptide epitope tag M2 and fluorescein isothiocyanate (FITC)-conjugated mouse anti-Flag M2, Sigma-Aldrich; rabbit anti-Flag, Zymed Laboratories or Sigma-Aldrich; mouse anti-c-myc 9E10, Developmental Studies Hybridoma Bank at the University of Iowa; rabbit anti-c-myc A14, Santa Cruz Biotechnology; mouse anti-CD71 (transferrin receptor) T56/14, Leinco Technologies; Alexa Fluor 488 (A488)- and Alexa Fluor 596 (A596)-conjugated goat-anti-mouse IgG and goat anti-rabbit IgG and A488-conjugated cholera toxin subunit B, Molecular Probes; and tetramethylrhodamine isothiocyanate (TRITC)- and FITC-conjugated goat anti-mouse IgG and rhodamine Red-X-conjugated F_{ab} fragment of goat anti-rabbit IgG, Jackson ImmunoResearch Laboratories.

Expression Plasmids and MuSK Mutants. rMuSK was cloned via RT-PCR from mRNA isolated from rat skeletal muscle primary cultures treated under differentiation conditions for 3 days (generously provided by Dr. Ken Rosen, Caritas St. Elizabeth's Medical Center). cDNA was prepared with the 1st strand cDNA Synthesis Kit (Boehringer Mannheim), and full-length clones of rMuSK were amplified via PCR using primers against the beginning and end of the rMuSK coding sequence using the Expand High Fidelity PCR System (Boehringer Mannheim). PCR products were ligated into the EcoRI and XbaI sites of the pBK-CMVΔlac vector (Stratagene). All rMuSK mutants were constructed using PCR-based mutagenesis of the affected region followed by insertion of the mutant sequence into wild-type MuSK and were derived from an RT-PCR clone with sequence identical to the rMuSK GenBank sequence (accession number U34985) with one exception: a 10 amino acid insert at the first splice site between E209 and V210 (insert = EDSEPERDTK, analogous to the insert at this site in human MuSK reported in ref *7*). Each mutant also contained an epitope tag inserted after L34 (either myc, inserted sequence EQKLISEEDLNL, or Flag, DYKDDDDKV). For simplicity's sake, all constructs maintain the GenBank sequence amino acid numbering; that is, the 10 aa splice insert and the epitope tag are not counted in the numbering. Other than these two insertions, the amino acid sequences contained in each of the mutant constructs included in these studies are as follows (see Figure 4): wild-type, rMuSK1−868; rMuSK-K608A, rMuSK 1−868 with K608 mutated to A; rMuSK-Δendo$_{569-868}$, rMuSK 1−568; rMuSK-Δendo$_{525-868}$, rMuSK 1−524; rMuSK-Δendo$_{515-868}$, rMuSK 1−514; rMuSK-Δecto$_{45-485}$, rMuSK 1−44/486-868; rMuSK-Δecto$_{37-492}$, rMuSK 1−36/493−868; rMuSK-Δecto$_{45-485}$-Δendo$_{525-868}$, rMuSK 1−44/486-524; rMuSK-Δecto$_{37-492}$-Δendo$_{515-868}$, rMuSK 1−36/486-514; ss-ΔN_{23-48} -rMuSK, rMuSK 1−22/49−868; rMuSK-trkTM, rMuSK 1−492/rat trkB 429−453/rMuSK 515−868; (trkN_{1-48})-rMuSK, rat trkB 1−48/rMuSK 48−868; and (rMuSKN_{1-48})-trkB, rMuSK 1−48/rtrkB 47−802. The DNA sequence of the complete insert of each mutant was verified by nucleotide sequencing performed at the Harvard Medical School Biopolymer Facility.

pBK-CMVΔlac-tMuSK-myc (*22*) was provided by Dr. Rick Huganir, John Hopkins School of Medicine; pCMX-myc-trkB (myc inserted after residue 36, between the signal sequence and the first structural domain) (*23*) by Dr. Philip Barker, Montreal Neurological Institute, McGill University; and pCDM8-erbB4 (human) (*24*) by Dr. Gabriel Corfas, Children's Hospital, Harvard Medical School.

Cell Culture. Human embryonic kidney HEK293T (293T) cells were grown in 25 cm^2 flasks in high glucose DMEM supplemented with 10% FBS, 1× L-glutamine, 1 mM sodium pyruvate, and 1× penicillin/streptamycin. Flasks were incubated at 37 °C and 10% CO_2. QT-6 cells (a gift of Dr. Josh Sanes (*14*)) were grown in Medium 199 (Earle's) supplemented with 5% FBS, 1% DMSO, 10% Tryptose Phosphate Broth, and 1× penicillin/streptamycin and incubated at 37 °C and 5% CO_2.

For transient transfection, cells were plated onto UV-sterilized 12 mm circle cover slips treated with rat tail collagen Type I (Becton Dickinson) at a density to yield about 50% confluence the next day; confluence at the time of transfection ranged from 40 to 70%. Each cover slip was transfected with 0.5 μg DNA(s) using either the calcium phosphate method (*25*) or the Fugene-6 transfection reagent (Roche, protocol according to manufacturer's instructions using a DNA/lipid ratio of 1 μg:2.5 μL). Following transfection, cells were incubated in growth medium under standard conditions until the time of fixation and staining.

Immunocytochemistry. Transiently transfected 293T cells were fixed and immunostained anywhere from 18 to 36 h after transfection—usually 24 h. The standard protocol for labeling surface proteins was as follows: cells were fixed in 1% PFA in PBS for 20 min at room temperature, then blocked in a solution of 4% bovine serum albumin (BSA, Fraction V, Sigma), 10% goat serum, and 100 mM lysine (to quench any remaining free PFA) in PBS for 1 h at room temperature. The cover slips were transferred to a solution of the primary (1°) antibody in Ab dilution buffer (4% BSA and 10% goat serum in PBS) and incubated at room temperature for 1 h, then incubated in secondary (2°) antibody in Ab dilution buffer for 1 h at room temperature, and then mounted using Citifluor mounting medium (Ted Pella, Inc.) onto Superfrost/Plus microscope slides (Fisher).

To label total (internal and surface) cellular receptor, a permeabilization step of 10 min in 0.1% Triton X-100 in PBS at room temperature was added immediately before the blocking step. In experiments involving differential labeling of surface and internal components (Figure 2), fixation and 1° antibody incubation were followed by the permeabilization step, and then a repeat of blocking and incubation in a second 1° antibody before labeling with 2° antibodies.

We performed several control experiments to address whether the observed staining pattern was an artifact of the

experimental conditions (data not shown). The same clustered pattern was observed in live, unfixed cells and in cells fixed at 4 °C (a temperature at which endocytotic processes should be shut down), suggesting that the pattern is not a result of reorganizations occurring during fixation. To address the possibility that the clusters were a result of antibody-induced aggregation in incompletely fixed cells, MuSK distribution was characterized in cells more strongly fixed at 4% PFA, or with an F_{ab} fragment of the secondary antibody to eliminate one of the potential bivalent cross-linkers. In each case, there was no change in the degree or pattern of immunofluorescent surface clusters. Epitope-tagged MuSK protein was visualized using both mouse monoclonal and rabbit polyclonal antibodies against both the myc and Flag epitope tags, and untagged MuSK was visualized using rabbit polyclonal antibodies against an extracellular epitope. The observed fluorescence pattern was the same for all of these antibodies, showing that the pattern of staining was not a function of the specific antibody or epitope tags being used. Finally, we transfected the QT-6 fibroblast cell line used in previous studies (*22*) and found the same staining pattern seen in 293T cells, suggesting that the result is not cell-type-specific.

Fluorescence Microscopy and Image Editing. Immunofluorescently labeled samples were examined using a Nikon Eclipse E800 epifluorescence microscope fitted with a PlanFluor 100×/1.30 oil immersion lens (Nikon) and a 100 W mercury lamp (Chiu Technical Corp.) as a light source. FITC and A488 were visualized using a Nikon 91617-FITC/HYQ filter (excitation 460−500 nm, emission 515−560 nm). Rhodamine, TRITC, and A596 were visualized using a Nikon 96171-Rhod/CY3/HYQ filter (excitation 530−550 nm, emission 590−650 nm). Images were collected using the MicroMAX 5 MHz Digital Camera System (Princeton Instruments) and the Metamorph Imaging System software (Universal Imaging Corp.) in grayscale without scaling or background subtraction. Offline processing of these images (level adjustment or color rendering) was performed using Adobe Photoshop. Image level adjustment involved rescaling the range of lowest to highest pixel values in the original images to a range of 0−256. For comparison of double-labeled samples, grayscale images were pseudo-colored to either magenta or green by converting the image to RGB color mode, then filling the green channel with black (yielding a magenta image) or filling the red and blue channels with black (yielding green). Perfect overlap (in both position and intensity) of green and magenta yields white.

Quantitation of Clustering and Colocalization. For the quantitation of the distribution of cluster size and shape, the in-focus region of a grayscale image from a MuSK-expressing cell was thresholded using Metamorph such that the positive pixels most closely matched those that visually defined clusters within the image. Using the Metamorph Integrated Morphometry Analysis tool, we measured each distinct object's mean radius, total pixel area, shape coefficient, and average and total pixel intensity. Objects with a pixel area less than or equal to 5 were excluded, since these generally represented thresholding noise.

To quantitate colocalization, the same 100 × 100 pixel area was selected from the two grayscale images from fluorescein and rhodamine optics for a given cell and focal plane. Using Metamorph, we exported the pixel intensities of the 100 × 100 array in both images to Microsoft Excel. These arrays were digitized such that any pixel with a value equal to or higher than the value of the 1000th largest pixel intensity (i.e., the top 10% of pixels) was assigned a value of 1, and other pixels were assigned a value of 0. A 100 × 100 overlap array was then calculated by multiplying the two digitized values for each pixel. The total number of pixels with value 1 in the overlap array divided by the total number of pixels with value 1 in the original array (∼1000) yielded a value between 0 and 1, which when expressed as a percentage was the percent colocalization for that image. The values for n represent the number of 100 × 100 pixel arrays for which this calculation was performed for a given pair of coexpressed proteins. No more than one array was used from a single cell, and to the extent possible, cells were selected from experiments performed on different dates (in most cases the population represents images gathered from two to three different experiments).

Statistical Analysis. To assess whether there is a specific association between two proteins in our expression system, the probability that the observed amount of colocalization could have occurred for two randomly distributed proteins was estimated according to the following protocol. From each 100 × 100 array of digitized pixel values, every seventh pixel (in both the vertical and horizontal axes) was selected, yielding a subarray of 225 independent pixels. We assume that two pixels separated by at least six pixels can be considered independent since type 2 clusters are about six pixels in diameter, and larger type 3 clusters most likely represent aggregates of type 2 clusters. With these two subarrays representing the fluorescence signal in both channels of the same cell, the probability that the resulting number of overlapping ones ("double positive pixels") would occur given two independent samples was calculated using a Fisher's exact test, yielding a p value. The lower the p value, the less likely the two samples are independent, that is, the more likely there is a specific association. The subset of selected pixels was then shifted by (1, 1) and the same analysis performed. Five more iterations of this shift yielded a total of seven p values for a given 100 × 100 array. Since the probability of rejecting the null hypothesis for any one of these seven frames is necessarily less than the sum of all seven probabilities, this sum was used as an upper bound for the p value for the entire array and is the p value assigned to that array. This approach errs on the side of accepting a false null hypothesis (i.e., concluding independence when, in reality, there is specific association); in other words, it is conservative with respect to concluding that a specific association occurs.

An aggregate p value for a given pair of proteins was generated using the p values of each individual array within the sample according to the following formula (*26*):

$$F_n(\boldsymbol{p}) = \boldsymbol{p} \sum_{i=0}^{n-1} \frac{(-\ln \boldsymbol{p})^i}{i!}$$

where n = number of p values and $\boldsymbol{p}$ = product of all p values.

This combined p value, $F_n(\boldsymbol{p})$, represents the probability that all of the observed expression patterns for a given protein pair could have occurred if there was no specific association

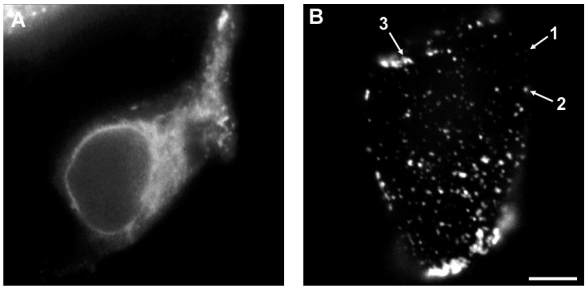

FIGURE 1: Transfected MuSK clusters at the surface of fibroblasts. Epifluorescence microscopy images of the distribution of transfected MuSK as visualized using antibodies against the extracellular myc epitope tag. (A) 293T cell fixed in 1% PFA and permeabilized in 0.1% Triton X-100 before antibody staining. (B) Cell fixed but not permeabilized to stain surface protein only. See text for discussion of the surface clusters represented by the arrows. Scale bar, 5 μm.

between the two proteins, and it is evaluated against a Bonferroni-corrected significance level of 0.002. It is the *p* value reported in Figure 9.

RESULTS

MuSK is Expressed in Discrete Clusters at the Cell Surface. Figure 1 shows the fluorescence pattern obtained from immunolabeling MuSK transfected into the fibroblast cell line HEK-293T (293T) under two experimental conditions. Cells that were fixed and permeabilized before antibody incubation, allowing for visualization of total cellular protein, had a diffuse, reticular pattern of staining that filled the cell, with a ring of strong perinuclear staining (presumably endoplasmic reticulum, Figure 1A). Cells that were fixed but not permeabilized, such that only the cell-surface MuSK but not internal MuSK would be labeled, had a markedly different pattern of staining made up of small, discrete puncta (Figure 1B). The camera exposure required to reach a given intensity level for permeabilized cells was as much as 10 times shorter than that required to reach the same intensity level for unpermeabilized cells. This difference in overall intensity suggests that the MuSK found in surface clusters represents a small fraction of the total MuSK in the cell. Images in all figures do not convey information about the relative absolute intensity between conditions because all images have been rescaled to the same maximum intensity (as described in Materials and Methods).

MuSK clustering at the cell surface was consistently observed in all 293T cells expressing the transfected protein. The immunofluorescent puncta could be classified in roughly three different categories based on size, identified with numbered arrows in Figure 1B. The most commonly observed was an intermediate-size cluster labeled as type 2; these puncta were typically round, on the order of 0.5 μm in diameter, and of moderate to strong fluorescence intensity (pixel intensities within the cluster were usually at least 5-fold higher than the intensity of pixels in areas of the cell surface between the clusters). Interspersed between the type 2 clusters were smaller grains of staining (type 1), which were up to 4-fold smaller in diameter and usually significantly dimmer, and larger irregularly shaped clusters (type 3), which were 2−5 times larger and usually of higher fluorescence intensity. Type 3 clusters often had the appearance of two or more type 2 clusters fused together. The mean cluster diameter

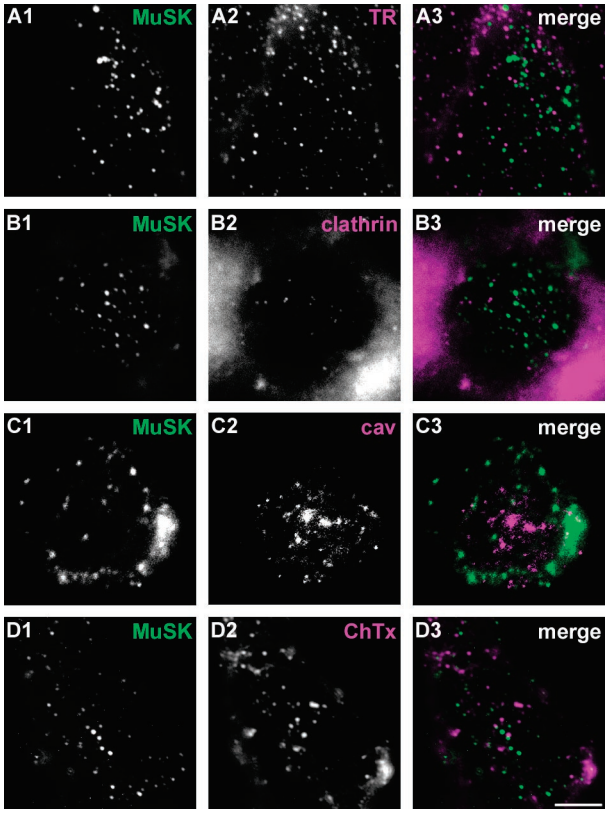

FIGURE 2: Transfected MuSK does not colocalize with cell compartment markers. 293T cells transfected with myc-tagged MuSK were stained for surface MuSK and for markers for cellular compartments, then visualized using epifluorescence microscopy. Image 1 in each row is the fluorescence signal for MuSK stained with an anti-epitope tag antibody. Image 2 in each row is the fluorescence for the cell compartment marker, stained as described below. Image 3 is the merge of images 1 and 2, pseudocolored. No significant overlap was seen for any of the markers tested, as visualized with (A) anti-transferrin receptor antibody, a marker for early endosomes; (B) anti-clathrin antibody, a marker for endocytotic clathrin-coated pits; (C) anti-caveolin antibody, a marker for caveolae; and (D) cholera toxin subunit B (ChTx), a marker for GM1 ganglioside-rich lipid rafts. Cells in panels A and D were fixed in 1% PFA and stained; cells in panels B and C were stained using the sequential staining protocol described in Materials and Methods for staining one surface protein and one internal protein. Scale bar, 5 μm.

for all clusters combined was 0.46 μm ($\pm$0.02 μm, $n = 212$ clusters), and the mean cluster area was 0.23 μm^2 ($\pm$0.02 μm^2, $n = 212$ clusters).

MuSK Does Not Colocalize with Cell Compartment Markers. One potential cause of the observed surface distribution was that the transfected protein was specifically targeted to some subcellular compartment. To test this, we double-labeled myc-MuSK-transfected 293T cells with anti-myc antibody and with markers for four different cellular compartments: anti-transferrin receptor antibody, a marker for surface-associated early endosomes (*27*); anti-clathrin antibody, a marker for clathrin-coated endocytotic pits (*28*); anti-caveolin antibody, a marker for caveolae (*18*); and cholera toxin B subunit, a marker for ganglioside-rich lipid rafts. As shown in Figure 2, in no instance did the immunofluorescent signal for MuSK overlap with the cell compartment marker. The punctate staining pattern, thus, is not a result of a cellular compartmentalization process, at least for the compartments tested.

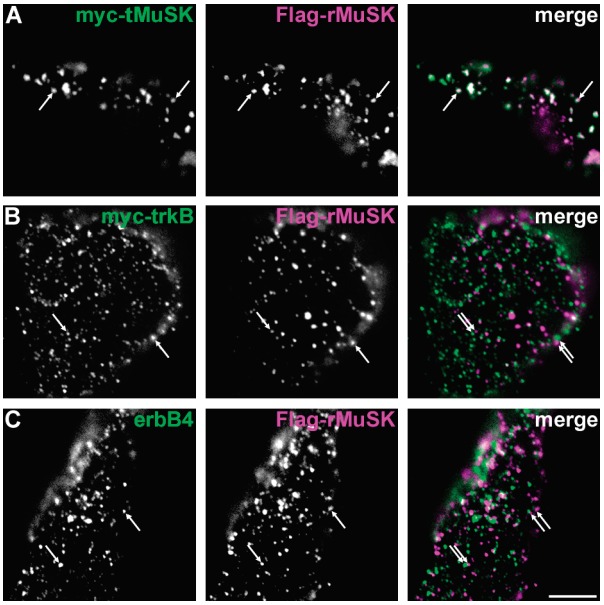

FIGURE 3: rMuSK clusters specifically with itself in 293T cells and not with cotransfected proteins. Flag-tagged rMuSK was cotransfected with other proteins containing a single membrane-spanning region, followed by immunostaining of the surface proteins and visualization using epifluorescence microscopy. (A) Surface clusters of myc-tMuSK (as visualized with an anti-myc antibody) and Flag-rMuSK (visualized with an anti-Flag antibody). The percent colocalization for coexpressed tMuSK and rMuSK was 70%, with $p < 10^{-5}$ (see text). (B) The surface clusters of myc-tagged rat trkB, visualized with anti-myc antibodies, have little or no overlap with clusters of coexpressed Flag-rMuSK. Percent colocalization was 18%, $p = 1.0$. (C) Clusters of coexpressed Flag-rMuSK and human erbB4 (visualized using an antibody against an extracellular region of erbB4) were segregated. Percent colocalization was 17%, $p = 1.0$. Scale bar, 5 μm.

MuSK Clustering Is Specific. We examined the surface distribution for several other single-pass transmembrane proteins in 293T cells, including transiently transfected RTKs trkB and erbB4 and the structural protein α/β-dystroglycan (all of which are also concentrated at the NMJ) and the endogenous proteins transferrin receptor and class I MHC. Each of these proteins had a clustered surface pattern in 293T cells. The only protein tested with a more uniform distribution at the cell surface was transfected CD4 (data not shown). These observations raised the possibility that the clusters were a result of a nonspecific aggregation of proteins expressed at a high level at the cell surface.

Coexpression studies, however, indicate that these proteins specifically self-associate and do not associate with other cotransfected proteins (Figure 3). *Torpedo* MuSK (tMuSK) and rat MuSK (rMuSK), tagged with different epitopes for differential labeling, exhibited immunofluorescence signals with a high degree of overlap (Figure 3A, see arrows). In contrast, when Flag-tagged rMuSK was coexpressed with either myc-trkB or erbB4, there was very little overlap between the two immunofluorescence signals, even though the clusters of the two proteins were intermingled and often in close proximity to each other (Figure 3B,C, see arrows for examples of neighboring but nonoverlapping clusters).

To quantitate the extent of overlap for two fluorescence images (and by inference two expressed proteins), we used an algorithm adapted from that used in ref *29*, as described in Materials and Methods. When this algorithm was used,

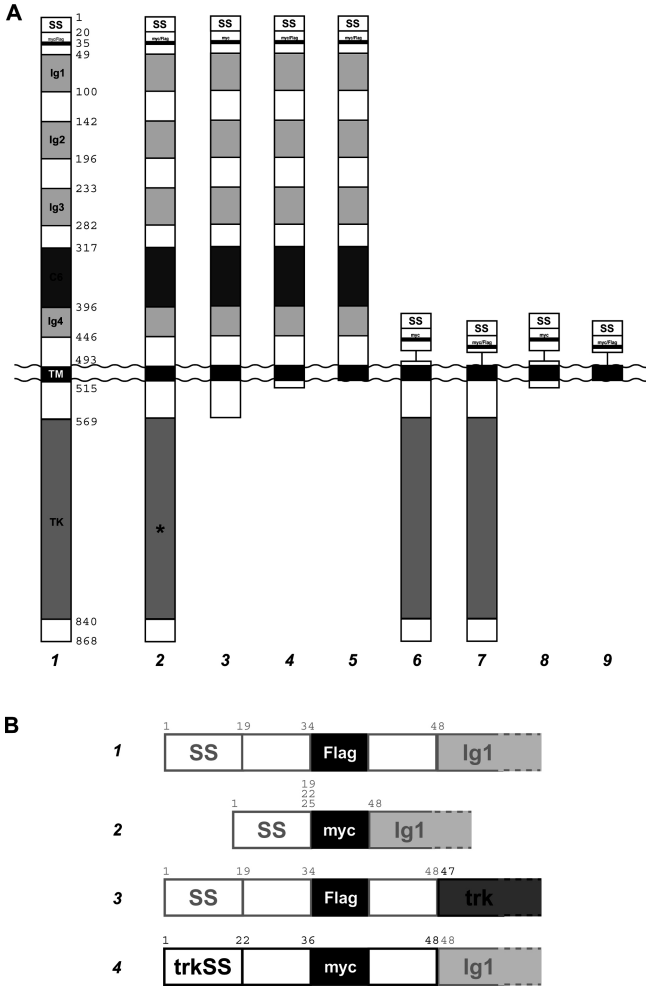

FIGURE 4: Cartoons of MuSK mutants. (A) Depiction of rat MuSK deletion mutants used. 1, wild-type; 2, rMuSK-K608A; 3, rMuSKΔendo$_{569-868}$; 4, rMuSK-Δendo$_{525-868}$; 5, rMuSK-Δendo$_{515-868}$; 6, rMuSK-Δecto$_{45-485}$; 7, rMuSK-Δecto$_{37-492}$; 8, rMuSK-Δecto$_{45-485}$-Δendo$_{525-868}$; and 9, rMuSK-Δecto$_{37-492}$-Δendo$_{515-868}$. (B) Depiction of deletions and substitutions at the rMuSK N-terminus, used in the experiments described in Figure 8. 1, wild-type; 2, myc-ss-ΔN$_{23-48}$-rMuSK (see text for explanation of the three different signal sequence endpoints); 3, Flag-(rMuSKN$_{1-48}$)-trkB; and 4, myc-(trkN$_{1-48}$)-rMuSK.

the calculated percent colocalization for coexpressed tMuSK and rMuSK was 70%. Statistical testing of the data using Fisher's exact test, as described in Materials and Methods, yields a probability of less than 10^{-5} that the distributions of these two proteins are independent of each other, indicating that there is a specific association between the two. The coexpressed pairs of rMuSK with either trkB or erbB4, however, yielded a percent colocalization of ~20%, with a p value of 0.9−1.0, indicating that the distributions of clusters of the two proteins are independent of each other.

Such prominent segregation of surface clusters of different proteins suggests that the punctate distribution is not a result of a nonspecific aggregation or cellular shepherding of overexpressed proteins at the cell surface and implies that MuSK self-association is specific.

Mutational Analysis: Extracellular and Intracellular Regions. To identify domains within the MuSK protein important for self-association, we engineered a panel of rMuSK mutants, as described in Materials and Methods. A cartoon of these rMuSK mutants is found in Figure 4.

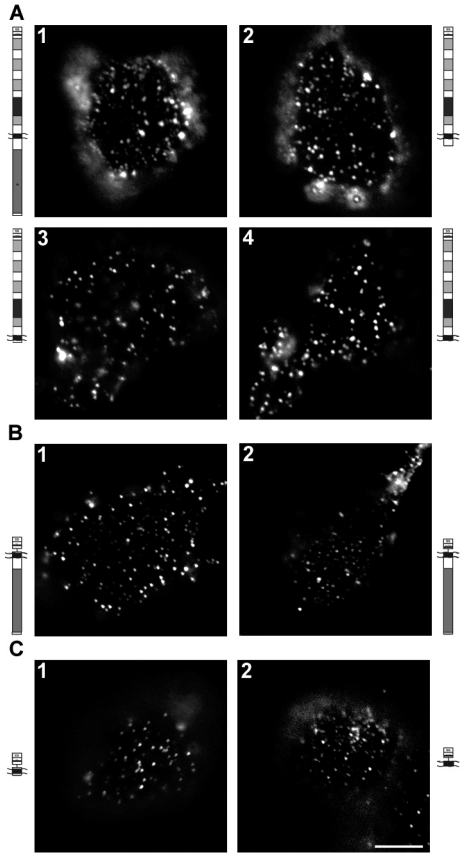

FIGURE 5: Neither the intracellular domain of rMuSK nor most of the extracellular region is necessary for clustering. 293T cells were transfected with a single rMuSK mutant, and the surface expression pattern was determined by immunofluorescent staining of the epitope tag in fixed cells. (A) rMuSK mutants with kinase-inactivating mutations or intracellular deletions were clustered. 1, myc-rMuSK−K608A; 2, myc-rMuSKΔendo$_{569-868}$; 3, myc-rMuSK-Δendo$_{525-868}$; and 4, myc-rMuSK−Δendo$_{515-868}$. (B) rMuSK mutants involving deletion of most of the extracellular domain, including all four Ig-like domains and the C6 box, were clustered. 1, myc-rMuSK-Δecto$_{45-485}$; and 2, Flag-rMuSK-Δecto$_{37-492}$. (C) rMuSK mutants combining both the intracellular and extracellular domain deletions were clustered. 1, myc-rMuSK-Δecto$_{45-485}$-Δendo$_{525-868}$; and 2, Flag-rMuSK-Δecto$_{37-492}$-Δendo$_{515-868}$. Scale bar, 5 μm.

Initially, we made large deletions in the intracellular domain of rMuSK by introducing premature stop codons either immediately before the kinase domain (Figure 4A, no. 3, rMuSKΔendo$_{569-868}$), 10 amino acids beyond the putative transmembrane (TM)-spanning region (Figure 4A, no. 4, rMuSKΔendo$_{525-868}$), or immediately after this TM domain (Figure 4A, no. 5, rMuSKΔendo$_{515-868}$). We also tested a full-length but kinase-inactive point mutant (*10*) (Figure 4A, no. 2, rMuS*K*$_{K608A}$). As shown in Figure 5A, each of these mutants was expressed in a clustered pattern at the surface of transfected 293T cells.

We also expressed two ectodomain deletions, removing either the region from Ig1−Ig4 (Figure 4A, no. 6, rMuSKΔecto$_{45-485}$) or more completely the entire sequence from just after the epitope tag to the beginning of the TM domain (Figure 4A, no. 7, rMuSKΔecto$_{37-492}$). Surface clusters were observed when these constructs were transfected into 293T cells (Figure 5B). Further, the endodomain and ectodomain deletions were combined in two constructs that retained only the N-terminus of the protein and the region of the TM domain (Figure 4A, nos. 8 and 9, rMuSKΔendo$_{525-868}$Δecto$_{45-485}$ and rMuSKΔendo$_{515-868}$Δecto$_{37-492}$). These minimal constructs were expressed at the surface of 293T cells in clusters (Figure 5C). Therefore, neither the entire intracellular domain nor the bulk of the extracellular domain is required for surface self-association to occur.

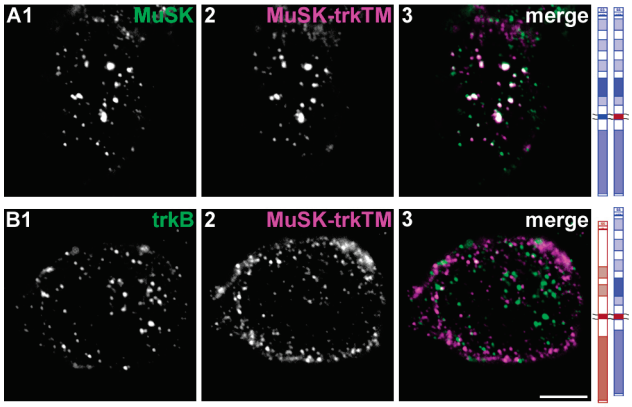

FIGURE 6: The transmembrane domain of MuSK is neither necessary nor sufficient for self-association. The transmembrane region (TM domain) of rMuSK was replaced with the TM domain of trkB (rMuSK-trkTM). This construct was coexpressed in 293T cells with either rMuSK or trkB. The pattern of surface expression was determined using immunofluorescence, and a percent colocalization was determined as described in Materials and Methods. (A) rMuSK lacking the rMuSK TM domain (rMuSK-trkTM, A2) was expressed at the surface in clusters similar to those seen for wild-type rat MuSK (A1). This chimera also had a high degree of colocalization (percent colocalization 61%, $p < 10^{-5}$) with clusters of wt rMuSK. (B) rMuSK-trkTM clusters were not colocalized with trkB clusters (18%, $p = 0.9$). Scale bar, 5 μm.

Mutational Analysis: The Transmembrane-Spanning Region of rMuSK. The question remained whether the TM domain, present in all constructs tested in Figure 5, might play a role in surface clustering. Since deletion of this TM domain would disrupt rMuSK's insertion into the membrane, we substituted the rat trkB TM domain for the rMuSK TM domain (rMuSK-trkTM). When expressed in 293T cells, rMuSK-trkTM was distributed in clusters at the surface. When this chimera was coexpressed with wild-type (wt) rMuSK, there was a high amount of colocalization of the clusters (61%, $p < 10^{-5}$, Figure 6A), indicating that the rMuSK TM domain is not necessary for association with rMuSK clusters. In addition, coexpression of rMuSK-trkTM with trkB in 293T cells resulted in clusters of each protein but with a low level of colocalization (18%, $p = 0.9$, Figure 6B). The trkB TM domain, thus, is not sufficient to recruit the chimera to trkB clusters.

Mutational Analysis: The rMuSK N-Terminus. The only region of rMuSK unaltered in all previously tested constructs was the N-terminal 36 amino acids, including the epitope tag. As illustrated in Figure 7, one set of coexpression studies performed with the rMuSK ectodomain deletion mutants had already suggested that the position of this N-terminus might be important in clustering. As previously shown, wt rMuSK and tMuSK surface clusters were highly colocalized when coexpressed in 293T cells (70%, $p < 10^{-5}$, Figure 7A). However, when wt rMuSK was coexpressed with the ectodomain deletion rMuSKΔecto$_{37-492}$, each was clustered at the surface with little colocalization (24%, $p = 0.6$,

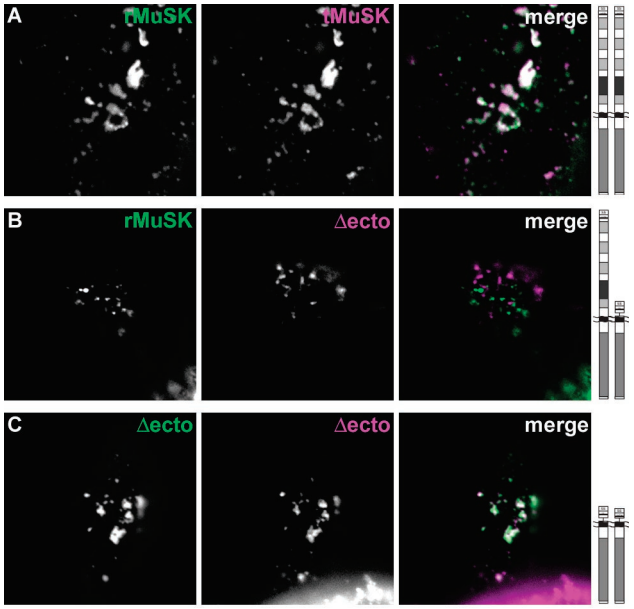

FIGURE 7: The relative position of the N-terminus affects rMuSK self-association. Pairwise cotransfections of rMuSK mutants were performed in 293T cells, followed by immunofluorescent visualization of surface protein expression and calculation of percent colocalization. (A) myc-rMuSK and Flag-rMuSK were highly colocalized (71%, $p < 10^{-5}$). (B) When Flag-rMuSK and myc-rMuSKΔecto$_{37-392}$ were coexpressed, almost no overlap was observed between the clusters of the two proteins (24%, $p = 0.9$). (C) Two differentially tagged Δecto rMuSKs, myc-rMuSKΔecto$_{37-392}$ and Flag-rMuSKΔecto$_{37-392}$, were colocalized (56%, $p < 10^{-5}$). Scale bar, 5 μm.

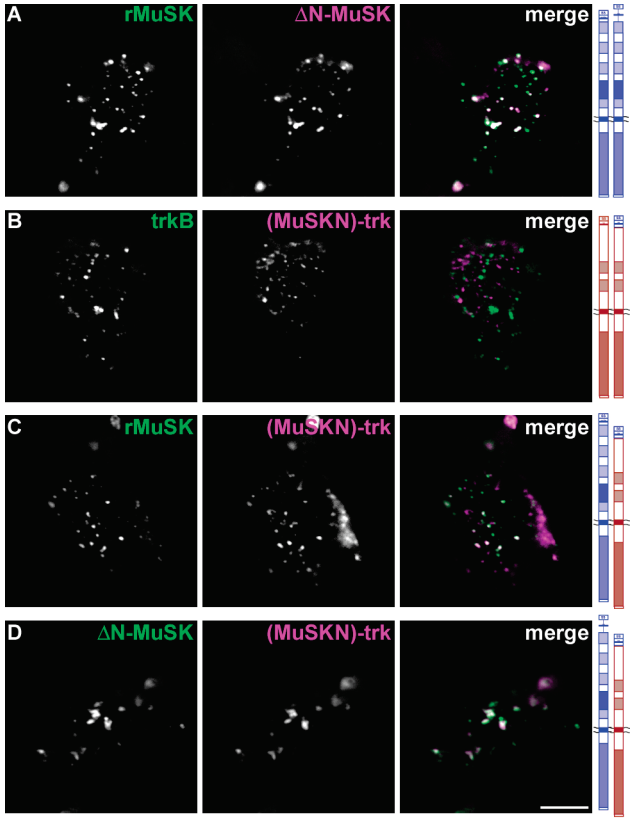

FIGURE 8: Colocalization of MuSK N-terminal mutants and chimeras. 293T cells expressing pairs of mutants were fixed, immunostained, and visualized, and the percent colocalization was calculated as previously described. (A) Flag-rMuSK + myc-ss-ΔN$_{23-48}$-rMuSK. Deletion of the post-signal sequence region around the epitope tag of rMuSK did not affect colocalization with wild-type rMuSK (68%, $p < 10^{-5}$). (B) myc-trkB + Flag-(rMuSKN$_{1-48}$)-trkB. Replacement of trkB's N-terminus with that of rMuSK abolished coclustering with trkB (25%, $p = 0.7$). (C) myc-rMuSK + Flag-(rMuSKN$_{1-48}$)-trkB. trkB, which normally is segregated at the surface from rMuSK, was recruited to wt rMuSK clusters upon substitution of its N-terminus with that of rMuSK (70%, $p < 10^{-5}$). (D) ss-ΔN$_{23-48}$-rMuSK + Flag-(rMuSKN$_{1-48}$)-trkB. Two mutants whose only common sequence is rMuSK 1−22 were highly colocalized (75%, $p < 10^{-5}$). Scale bar, 5 μm.

Figure 7B). A return to a more colocalized distribution was seen when two differentially labeled ectodomain mutant rMuSKs were coexpressed (56%, $p < 10^{-5}$, Figure 7C). Hence, colocalization occurred when the N-termini of the two proteins were at the same position in relation to the membrane (Figure 7A,C) but was abolished when the relative positions of the N-termini were offset (Figure 7B).

To assay the role of the N-terminal sequences of rMuSK without eliminating a signal sequence or epitope tag, we constructed the deletion mutants and chimeras illustrated in Figure 4B. The three ss-ΔN$_{x-48}$-rMuSK mutants deleted the latter half of this N-terminus while keeping the signal sequence and the epitope tag (Figure 4B, no. 2). Three ΔN mutants were made, retaining the first 19, 22, and 25 amino acids of the rMuSK coding sequence because of uncertainty as to the minimum sequence required for proper presumed signal sequence processing. In addition, chimeras were made in which the N-termini of trkB and rMuSK were swapped ((MuSKN$_{1-48}$)-trkB and (trkN$_{1-48}$)-rMuSK, Figure 4B, nos. 3 and 4).

Both ss-ΔN$_{26-48}$-rMuSK and ss-ΔN$_{23-48}$-rMuSK were clustered at the surface when expressed in 293T cells. The ss-ΔN$_{20-48}$-rMuSK construct was expressed internally but never reached the surface plasma membrane, suggesting that at least the first 20−22 residues are required for proper membrane insertion and transport to the surface (data not shown). When ss-ΔN$_{23-48}$-rMuSK was coexpressed with wt rMuSK, there was a high degree of colocalization (68%, $p < 10^{-5}$, Figure 8A); this result was the same for ss-ΔN$_{26-48}$-rMuSK (data not shown). That the ss-ΔN-rMuSK constructs were themselves clustered and that they colocalized with wt MuSK clusters suggest that the region of the N-terminus following the putative signal sequence (residues 23−48) is unnecessary for self-association.

The entire N-terminal region (residues 1−45) as a whole, however, is involved in self-association. Replacing the N-terminus of trkB with that of rMuSK yielded a protein ((MuSKN$_{1-48}$)-trkB) whose surface clusters no longer colocalized with those of wt trkB (24%, $p = 0.9$, Figure 8B). In addition, the rMuSK N-terminus confers the ability to associate with wt rMuSK clusters, as coexpressed (MuSKN$_{1-48}$)-trkB and wt rMuSK were highly colocalized (70%, $p < 10^{-5}$, Figure 8C). Thus, the N-terminal 48 amino acids of rMuSK are sufficient to recruit the trkB protein to rMuSK clusters.

Given that the rMuSK N-terminus is sufficient for association of trkB with rMuSK clusters (Figure 8B) but the latter half of this N-terminus is not necessary for coclustering (Figure 8A), the first 22 amino acids—the putative signal sequence—are implicated in self-association. This is supported by the fact that surface clusters of (MuSKN$_{1-48}$)-trkB and those of ss-ΔN$_{23-48}$-rMuSK were highly colocalized (73%, $p < 10^{-5}$, Figure 8D). In this instance, the N-terminus of rMuSK is sufficient to allow colocalization with a protein

A

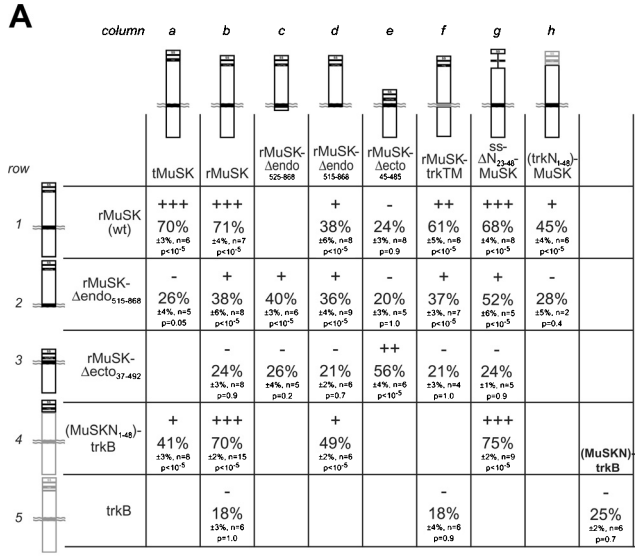

B

rat MuSK	**M**REL-**VNIPL**VH**IL**TLVAF**S**GT EK-**LPKAP**VI
***Torpedo* MuSK**	**M**NFIP**VDIPL**LM**IL**LVTTG**S**SA DGI**LPKAP**QI
rat trkB	MARLWGLCLLVLGFWRASLA CPMSCKCSTT

FIGURE 9: Analysis of colocalization and signal sequences. (A) Summary of the results of colocalization studies in 293T cells for pairs of MuSK mutants/chimeras. Each cell presents the summary data for the quantitated coexpression of the two corresponding proteins and is presented as mean ± SEM, with the number of quantitated samples. Beneath that is the aggregate *p* value calculated using the combined individual *p* values from each sample (see Materials and Methods). Empty cell, pair not quantitated. − = <33%; + = 33−50%; ++ = 50−67%; +++ = >67%. (B) Alignment of the N-terminal amino acid sequences for rMuSK, tMuSK, and trkB. The break in the sequence indicates the predicted site of signal peptide cleavage (using the SignalP 3.0 algorithm, http://www.cbs.dtu.dk/services/SignalP).

that has the signal sequence of rMuSK but not the remaining sequence preceding the first Ig-like domain.

DISCUSSION

We used a mutational analysis to identify domains within MuSK necessary for self-association. Figure 9 summarizes the colocalization results for all of the tested protein pairs. Each box within the chart displays the mean percent colocalization for the corresponding protein pair for the number of cells quantitated. The results are binned into four categories: "-", indicating no observable specific association of the clusters of the two proteins and insignificant aggregate *p* values, and "+" to "+++", indicating significant aggregate *p* values and increasing degree of observed colocalization.

The predicted signal sequence (specifically residues 1−22) plays an essential role in MuSK self-association. This region is sufficient to confer recruitment to MuSK clusters, based on the strong colocalization of ss-ΔN_{23-48}-rMuSK and ($MuSKN_{1-48}$)-trkB (75% colocalization, $p < 10^{-5}$, Figure 9, box 4g). The importance of this region explains why pairs of proteins in which the N-termini are distant from each other, relative to the plane of the membrane, do not colocalize (21−26%, $p > 0.1$, Figure 9A, boxes 3b−d,f,g). As shown in Figure 9B, there is a high degree of homology in the predicted signal sequences of rMuSK and tMuSK, which strongly colocalize, and no observable homology between those of rMuSK and trkB, which do not colocalize.

At this point it remains unclear how the signal sequence might promote and/or maintain clustering. The standard model for membrane insertion of integral membrane proteins predicts that the signal sequence is cleaved, and for those proteins that have been studied, it appears this cleavage is cotranslational and occurs shortly after the signal sequence emerges from the translocon into the lumen of the ER (*30*, *31*). It is not known whether, and if so where, the signal sequence is cleaved in the mature MuSK protein. This is the subject of an ongoing investigation in our lab. The signal sequences of the EGF, insulin, and PDGF RTKs are cleaved in the mature protein, based on N-terminal sequencing performed during their original purification (*32*−*34*).

If signal peptide cleavage occurs for MuSK in these cells, promotion of clustering at the cell surface could not occur via protein−protein interactions involving the signal sequence at the cell surface. One plausible mechanism for a cleaved signal sequence to induce clustering would be that the signal sequence targets the nascent MuSK peptide to a specific subcompartment of the ER, and that this subcompartment directs MuSK into a trafficking pathway that processes the protein in a way that results in cluster formation. This mechanism would be in agreement with the evolving notion that signal peptides may be involved in specific targeting beyond just membrane insertion (*31*). If this were the case though, one would have to postulate the existence of several different ER compartments, or different trafficking pathways, to account for the self-specificity of clustering for several proteins, and currently, there is no evidence for such a multiplicity of parallel trafficking pathways.

Another possibility is that the signal peptide of MuSK is not cleaved and remains as a part of the mature protein. In this case, some sort of direct homophilic interaction between neighboring signal peptides could account for clustering, or alternatively, a cluster could result from an interaction of the peptide with other proteins that are associated with the plasma membrane or the extracellular matrix. Any interaction with other cellular proteins would not involve muscle-specific proteins, since the clustering occurs in fibroblasts. The maintenance of the signal peptide in a mature integral membrane protein has been reported (*35*), but we are not aware of any experiments demonstrating retention of the signal peptide for any RTK.

The colocalization studies summarized in Figure 9 also establish that the intracellular domain of MuSK, while not required for clustering, strengthens association. Deletion of the entire endodomain, in rMuSKΔendo$_{515-868}$, does not abolish surface clustering of the rMuSK protein (Figure 5A). However, quantitation of the amount of colocalization between this deletion mutant and other MuSK mutants shows that colocalization is weakened without the endodomain (Figure 9A, row 2). There is specific association of rMuSKΔendo$_{515-868}$ with wild-type MuSK or other endodomain mutants, as indicated by the significant aggregate *p* values, but the colocalization values are relatively low (35−40%, $p < 10^{-5}$, Figure 9A, box 2b−d). It may be that the interactions between neighboring endodomains within the cluster have an enhancing effect on cluster formation or maintenance. This could be a specific interaction between

MuSK endodomains, or perhaps could be a property of any kinase domains in close proximity to each other. Alternatively, the endodomain may stabilize clusters through interactions with other cellular proteins. MuSK is known to interact with cytoskeleton-associated proteins (*36*−*38*), and such endodomain interactions might play a role in our system. Paradoxically, when two identical rMuSKΔendo$_{515-868}$ mutants with different epitope tags are coexpressed, the clusters of the two are only mildly associated (36%, $p < 10^{-5}$, Figure 9A, box 2d). The lack of cluster intermingling in this instance raises the possibility that clusters of proteins translated from different sources are initially segregated before reaching the surface, and that maintenance of this segregation at the surface accounts in part for the lack of coclustering of different proteins. In this scenario, the endodomain might play a role in allowing the association of clusters once they have reached the surface.

The implication that MuSK plays a structural role at the NMJ in addition to its function as a signaling molecule (*14*) distinguishes it from other RTKs, and MuSK self-association might contribute to that structural role. Alternatively, MuSK clustering may have a function that is common to most RTKs, since receptor clustering is not unique to MuSK. In fact, almost every single-pass transmembrane protein we tested, endogenous or exogenous, had a similar punctate distribution. Surface clusters of similar size have been reported for other RTKs, such as members of the erbB and Eph receptor families (*39*, *40*). How RTK function in general is affected by clustering, and if such effects are the same for every RTK, remains unclear.

Studies of membrane protein localization in cultured fibroblast cell lines are performed under the assumption that the results are relevant to that protein in its native environment. While this technique has been used widely, different interactions are seen for caveolin isoforms when expressed in muscle cells compared with fibroblasts (*41*). In an effort to test this assumption in the case of MuSK, we tried to characterize the surface distribution of MuSK in the C2C12 skeletal muscle cell line. However, none of the anti-MuSK antibodies that we tested yielded a fluorescent signal above background in C2C12 cultures, in both myoblasts and differentiated myotubes, naïve or agrin-treated. Similarly, transfected C2C12 cells expressing exogenous MuSK had no surface MuSK signal, using either anti-MuSK or anti-epitope tag antibodies. These cells expressed transfected MuSK protein internally, as visualized in permeabilized cells, but any protein at the surface was undetectable (data not shown).

Further research is necessary to elucidate the mechanisms by which the signal sequence promotes clustering and the endodomain strengthens it. The results of such experiments would have significant implications not only for MuSK clustering and MuSK function but also for our understanding of signal sequence function and processing and the trafficking of RTKs.

REFERENCES

1. Sanes, J. R., and Lichtman, J. W. (2001) Induction, Assembly, Maturation and Maintenance of a Postsynaptic Apparatus, *Nat. Rev. Neurosci. 2*, 791−805.
2. Salpeter, M. M., and Loring, R. H. (1985) Nicotinic Acetylcholine Receptors in Vertebrate Muscle: Properties, Distribution and Neural Control, *Prog. Neurobiol. 25*, 297−325.
3. Salpeter, M. M., Marchaterre, M., and Harris, R. (1988) Distribution of Extrajunctional Acetylcholine Receptors on a Vertebrate Muscle: Evaluated by Using a Scanning Electron Microscope Autoradiographic Procedure, *J. Cell Biol. 106*, 2087−2093.
4. Merlie, J. P. (1984) Biogenesis of the Acetylcholine Receptor, a Multisubunit Integral Membrane Protein, *Cell 36*, 573−575.
5. Denzer, A. J., Hauser, D. M., Gesemann, M., and Ruegg, M. A. (2004) Synaptic Differentiation: the Role of Agrin in the Formation and Maintenance of the Neuromuscular Junction, *Cell Tissue Res. 290*, 357−365.
6. Gautam, M., Noakes, P. G., Moscoso, L., Rupp, F., Scheller, R. H., Merlie, J. P., and Sanes, J. R. (1996) Defective Neuromuscular Synaptogenesis in Agrin-Deficient Mutant Mice, *Cell 85*, 525−535.
7. Valenzuela, D. M., Stitt, T. N., Distefano, P. S., Rojas, E., Mattsson, K., Compton, D. L., Nunez, L., Park, J. S., Stark, J. L., Gies, D. R., Thomas, S., Lebeau, M. M., Fernald, A. A., Copeland, N. G., Jenkins, N. A., Burden, S. J., Glass, D. J., and Yancopoulos, G. D. (1995) Receptor Tyrosine Kinase Specific for the Skeletal Muscle Lineage: Expression in Embryonic Muscle, at the Neuromuscular Junction, and After Injury, *Neuron 15*, 573−584.
8. Glass, D. J., Bowen, D. C., Stitt, T. N., Radziejewski, C., Bruno, J., Ryan, T. E., Gies, D. R., Shah, S., Mattsson, K., Burden, S. J., Distefano, P. S., Valenzuela, D. M., Dechiara, T. M., and Yancopoulos, G. D. (1996) Agrin Acts via a MuSK Receptor Complex, *Cell 85*, 513−523.
9. Dechiara, T. M., Bowen, D. C., Valenzuela, D. M., Simmons, M. V., Poueymirou, W. T., Thomas, S., Kinetz, E., Compton, D. L., Rojas, E., Park, J. S., Smith, C., Distefano, P. S., Glass, D. J., Burden, S. J., and Yancopoulos, G. D. (1996) The Receptor Tyrosine Kinase MuSK Is Required for Neuromuscular Junction Formation in Vivo, *Cell 85*, 501−512.
10. Hopf, C., and Hoch, W. (1998) Dimerization of the Muscle-Specific Kinase Induces Tyrosine Phosphorylation of Acetylcholine Receptors and Their Aggregation on the Surface of Myotubes, *J. Biol. Chem. 273*, 6467−6473.
11. Hopf, C., and Hoch, W. (1997) Heparin Inhibits Acetylcholine Receptor Aggregation at Two Distinct Steps in the Agrin-Induced Pathway, *Eur. J. Neurosci. 9*, 1170−1177.
12. Willmann, R., and Fuhrer, C. (2002) Neuromuscular Synaptogenesis: Clustering of Acetylcholine Receptors Revisited, *Cell. Mol. Life Sci. 59*, 1296−1316.
13. Glass, D. J., Apel, E. D., Shah, S., Bowen, D. C., Dechiara, T. M., Stitt, T. N., Sanes, J. R., and Yancopoulos, G. D. (1997) Kinase Domain of the Muscle-Specific Receptor Tyrosine Kinase (MuSK) Is Sufficient for Phosphorylation but Not Clustering of Acetylcholine Receptors: Required Role for the MuSK Ectodomain?, *Proc. Natl. Acad. Sci. U.S.A. 94*, 8848−8853.
14. Apel, E. D., Glass, D. J., Moscoso, L. M., Yancopoulos, G. D., and Sanes, J. R. (1997) Rapsyn Is Required for MuSK Signaling and Recruits Synaptic Components to a MuSK-Containing Scaffold, *Neuron 18*, 623−635.
15. Gautam, M., Dechiara, T. M., Glass, D. J., Yancopoulos, G. D., and Sanes, J. R. (1999) Distinct Phenotypes of Mutant Mice Lacking Agrin, MuSK, or Rapsyn, *Dev. Brain Res. 114*, 171−178.
16. Trinidad, J. C., Fischbach, G. D., and Cohen, J. B. (2000) The Agrin/MuSK Signaling Pathway Is Spatially Segregated From the Neuregulin/ErbB Receptor Signaling Pathway at the Neuromuscular Junction, *J. Neurosci. 20*, 8762−8770.
17. Pike, L. J. (2003) Lipid Rafts: Bringing Order to Chaos, *J. Lipid Res. 44*, 655−667.
18. van Deurs, B., Roepstorff, K., Hommelgaard, A. M., and Sandvig, K. (2003) Caveolae: Anchored, Multifunctional Platforms in Thelipid Ocean, *Trends Cell Biol. 13*, 92−100.
19. Ceresa, B. P., and Schmid, S. L. (2000) Regulation of Signal Transduction by Endocytosis, *Curr. Opin. Cell Biol. 12*, 204−210.
20. Herbst, R., and Burden, S. J. (2000) The Juxtamembrane Region of MuSK Has a Critical Role in Agrin-Mediated Signaling, *EMBO J. 19*, 67−77.
21. Zhou, H., Glass, D. J., Yancopoulos, G. D., and Sanes, J. R. (1999) Distinct Domains of MuSK Mediate Its Abilities to Induce and to Associate With Postsynaptic Specializations, *J. Cell Biol. 146*, 1133−1146.
22. Gillespie, S. K. H., Balasubramanian, S., Fung, E. T., and Huganir, R. L. (1996) Rapsyn Clusters and Activates the Synapse-Specific Receptor Tyrosine Kinase MuSK, *Neuron 16*, 953−962.

23. Kryl, D., Yacoubian, T., Haapasalo, A., Castren, E., Lo, D., and Barker, P. A. (1999) Subcellular Localization of Full-Length and Truncated Trk Receptor Isoforms in Polarized Neurons and Epithelial Cells, *J. Neurosci. 19*, 5823−5833.
24. Elenius, K., Corfas, G., Paul, S., Choi, C. J., Rio, C., Plowman, G. D., and Klagsbrun, M. (1997) A Novel Juxtamembrane Domain Isoform of HER4/ErbB4. Isoform-Specific Tissue Distribution and Differential Processing in Response to Phorbol Ester, *J. Biol. Chem. 272*, 26761−26768.
25. Ramarao, M. K., and Cohen, J. B. (1998) Mechanism of Nicotinic Acetylcholine Receptor Cluster Formation by Rapsyn, *Proc. Natl. Acad. Sci. U.S.A. 95*, 4007−4012.
26. Bailey, T. L., and Gribskov, M. (1998) Combining Evidence Using P-Values: Application to Sequence Homology Searches, *Bioinformatics 14*, 48−54.
27. Dautry-Varsat, A. (1986) Receptor-Mediated Endocytosis: The Intracellular Journey of Transferrin and Its Receptor, *Biochimie 68*, 375−381.
28. Brodsky, F. M. (1985) Clathrin Structure Characterized with Monoclonal Antibodies. II. Identification of in Vivo Forms of Clathrin, *J. Cell Biol. 101*, 2055−2062.
29. Carter, A. R., Chen, C., Schwartz, P. M., and Segal, R. A. (2002) Brain-Derived Neurotrophic Factor Modulates Cerebellar Plasticity and Synaptic Ultrastructure, *J. Neurosci. 22*, 1316−1327.
30. Keenan, R. J., Freymann, D. M., Stroud, R. M., and Walter, P. (2001) The Signal Recognition Particle, *Annu. Rev. Biochem. 70*, 755−775.
31. Stroud, R. M., and Walter, P. (1999) Signal Sequence Recognition and Protein Targeting, *Curr. Opin. Struct. Biol. 9*, 754−759.
32. Ullrich, A., Coussens, L., Hayflick, J. S., Dull, T. J., Gray, A., Tam, A. W., Lee, J., Yarden, Y., Libermann, T. A., Schlessinger, J., Downward, J., Mayes, E. L. V., Whittle, N., Waterfield, M. D., and Seeburg, P. H. (1984) Human Epidermal Growth Factor Receptor CDNA Sequence and Aberrant Expression of the Amplified Gene in A431 Epidermoid Carcinoma Cells, *Nature 309*, 418−425.
33. Ebina, Y., Ellis, L., Jarnagin, K., Edery, M., Graf, L., Clauser, E., Ou, J. H., Masiarz, F., Kan, Y. W., Goldfine, I. D., Roth, R. A., and Rutter, W. J. (1985) The Human Insulin Receptor CDNA: The Structural Basis for Hormone-Activated Transmembrane Signalling, *Cell 40*, 747−758.
34. Yarden, Y., Escobedo, J. A., Kuang, W. J., Yang-Feng, T. L., Daniel, T. O., Tremble, P. M., Chen, E. Y., Ando, M. E., Harkins, R. N., Francke, U., Fried, V. A., Ullrich, A., and Williams, L. T. (1986) Structure of the Receptor for Platelet-Derived Growth Factor Helps Define a Family of Closely Related Growth Factor Receptors, *Nature 323*, 226−232.
35. Gewurz, G. E., Ploegh, H. L., and Tortorella, D. (2002) US2, a Human Cytomegalovirus-Encoded Type I Membrane Protein, Contains a Non-Cleavable Amino-Terminal Signal Peptide, *J. Biol. Chem. 277*, 11306−11313.
36. Xia, J., Zhang, X., Staudinger, J., and Huganir, R. L. (1999) Clustering of AMPA Receptors by the Synaptic PDZ Domain-Containing Protein PICK1, *Neuron 22*, 179−187.
37. Strochlic, L., Cartaud, A., Labas, V., Hoch, W., Rossier, J., and Cartaud, J. (2001) MAGI-1c: A Synaptic MAGUK Interacting with MuSK at the Vertebrate Neuromuscular Junction, *J. Cell Biol. 53*, 1127−1132.
38. Luo, Z. G., Wang, Q., Zhou, J. Z., Wang, J. B., Luo, Z. J., Liu, M. Y., He, X., WynshawBoris, A., Xiong, W. C., Lu, B., and Mei, L. (2002) Regulation of AChR Clustering by Dishevelled Interacting With MuSK and PAK1, *Neuron 35*, 489−505.
39. Nagy, P., Jenei, A., Kirsch, A. K., Szollosi, J., Damjanovich, S., and Jovin, T. M. (1999) Activation-Dependent Clustering of the ErbB2 Receptor Tyrosine Kinase Detected by Scanning Near-Field Optical Microscopy, *J. Cell Sci. 112*, 1733−1741.
40. Torres, R., Firestein, B. L., Dong, H., Staudinger, J., Olson, E. N., Huganir, R. L., Bredt, D. S., Gale, N. W., and Yancopoulos, G. D. (1998) PDZ Proteins Bind, Cluster, and Synaptically Colocalize With Eph Receptors and Their Ephrin Ligands, *Neuron 21*, 1453−1463.
41. Capozza, F., Cohen, A. W., Cheung, M., Sotgia, F., Schubert, W., Battista, M., Lee, H., Frank, P. G., and Lisanti, M. P. (2005) Muscle-specific Interactions of Caveolin Isoforms: Differential Complex Formation between Caveolins in Fibroblastic vs. Muscle Cells, *Am. J. Physiol.: Cell Physiol. 288*, C677−C691.

BI051549J